www.czasopisma.pan.pl PAN POLSKA AKADEMIA NAUK www.journals.pan.pl

A R C H I V E S O F M E T A L L U R G Y A N D M A T E R I A L S

Volume 60 2015 Issue 2

DOI: 10.1515/amm-2015-0233

B. ŁYSOŃ-SYPIEŃ[*,♯], K. ZAKRZEWSKA[*], M. GAJEWSKA[**], M. RADECKA[***]

HYDROGEN SENSOR OF TiO_2-BASED NANOMATERIALS

SENSOR WODORU NA BAZIE NANOMATERIAŁÓW TiO_2

The aim of this research was to examine gas sensing properties of TiO_2 based nanomaterials. Nanopowders of Cr doped TiO_2 with constant Specific Surface Area, SSA, were obtained using Flame Spray Synthesis technique, FSS. Nanomaterials were characterized by Brunauer – Emmett – Teller adsorption isotherms, BET, X – ray diffraction, XRD, Transmission Electron Microscopy, TEM, optical spectrometry UV – vis with the use of an integrating sphere as well as impedance spectroscopy. Detection of hydrogen was carried out over the concentration range of 50 - 3000 ppm at the temperatures extending from 200 to 400°C and synthetic air working as a reference atmosphere. As a result of experiments it appeared that incorporation of 5 at.% of Cr into TiO_2 improved hydrogen sensing features due to small crystallite size and predominance of rutile polymorphic phase.

Keywords: TiO_2 nanomaterials, Cr dopant, hydrogen sensor

Przedmiotem pracy są nanomateriały na bazie TiO_2 do zastosowań sensorowych. Nanoproszki TiO_2 domieszkowane chromem o stałej powierzchni właściwej SSA (ang. Specific Surface Area) otrzymano przy pomocy techniki syntezy w płomieniu FSS (ang. Flame Spray Synthesis). Materiały poddano charakteryzacji z wykorzystaniem: izoterm adsorpcyjnych Brunauer – Emmett – Teller, BET, dyfraktometrii rentgenowskiej, XRD, transmisyjnej mikroskopii elektronowej, TEM, spektroskopii optycznej UV – vis oraz spektroskopii impedancyjnej. Pomiar własności sensorowych został przeprowadzony dla koncentracji H_2 w zakresie 50-3000 ppm w przedziale temperatur 200-400°C. Wykazano, że najlepiej na wodór odpowiada próbka TiO_2: 5at.% Cr charakteryzująca się małym rozmiarem krystalitów oraz przewagą fazy rutylu.

1. Introduction

Titanium dioxide is commonly used within different fields of science and industry due to its unique physical and chemical features such as high refractive index, thermal stability, high dielectric constant, non - toxicity, photocatalytic properties. Among many possible applications of TiO_2 one can specify: pigments (cosmetics, toothpaste, paints) [1, 2], self – cleaning and sterilizing surfaces [3, 4], water and air cleaning devices [5, 6], microelectronic devices [7, 8], food industry [9, 10], systems of solar energy conversion [11, 12], water splitting, hydrogen production and storage [13, 14], photochromic devices [15] and gas sensors [16-20].

The interest in TiO_2 based materials for resistive gas sensors began around 1980s due to the promising features such as: large and reversible changes in the electrical resistance along with the exceptional chemical stability. In order to improve TiO_2 sensor characteristics doping with metal ions can be applied. Recently, it has been reported that Cr addition improves sensitivity and response time of TiO_2 based sensors due to the increase in concentration of oxygen vacancies [21, 22]. It has been also proved that chromium additive affects anatase to rutile transformation [23-26]. The kinetics of this irreversible conversion is influenced by many factors, e.g., temperature, sample elaboration procedure, morphology, as well as impurities present in the structure [27]. According to Hanaor and Sorrell [27] the positive effect of Cr dopant on accelerating anatase to rutile transformation can be attributed to the additional oxygen vacancies which are formed upon substitutional incorporation of Cr^{3+} into TiO_2 lattice.

Furthermore, Cr dopant modifies electronic structure of TiO_2, influences its conductivity and can induce n to p transition as it was observed previously [28-32].

The aim of this work is to study the influence of Cr dopant on TiO_2 nanopowders used for H_2 sensing applications. The subject of our research is to study possible changes in crystallographic, electronic structure, electrical properties as well as gas sensing characteristics of TiO_2. Previously, our research on TiO_2: Cr took into account both the influence of grain size and dopant amount [33]. In this work, the grain size was controlled so as to study the impact of Cr concentration, only.

[*] AGH UNIVERSITY OF SCIENCE AND TECHNOLOGY, FACULTY OF COMPUTER SCIENCE, ELECTRONICS AND TELECOMMUNICATIONS, AL. A. MICKIEWICZA 30, 30-059 KRAKÓW, POLAND

[**] AGH UNIVERSITY OF SCIENCE AND TECHNOLOGY, ACADEMIC CENTER OF MATERIALS AND NANOTECHNOLOGY, ACMIN, AL. A. MICKIEWICZA 30, 30-059 KRAKÓW, POLAND

[***] AGH UNIVERSITY OF SCIENCE AND TECHNOLOGY, FACULTY OF MATERIALS SCIENCE AND CERAMICS, AL. A. MICKIEWICZA 30, 30-059 KRAKÓW, POLAND

[♯] Corresponding author: lyson@agh.edu.pl

2. Experimental

In order to synthesize Cr doped TiO_2 nanopowders with a controlled grain size, the Flame Spray Synthesis technique was used as described in [33]. Pure TiO_2 was obtained from titanium – 2.4 – pentanedionate ($C_{16}H_{28}O_6Ti$) dissolved in ethanol, whereas in the case of TiO_2: Cr titanium tetraisopropoxide $Ti(C_3H_7O)_4$ and chromium acetyloacetonate $C_{15}H_{21}CrO_6$ dissolved in m – xylene were used as metal organic precursors. In order to investigate the influence of Cr dopant only, Specific Surface Area, *SSA*, was kept constant at the level of about 60 m^2/g. However, in the case of TiO_2: 5 at.% Cr this objective was not reached due to the increased density of oxygen vacancies, which influence anatase to rutile transformation.

Brunauer – Emmett – Teller adsorption isotherm, BET, were obtained with Beckman – Coulter SA 3100 analyzer. BET technique was used to determine Specific Surface Area, SSA, from which the equivalent particle diameter, d_{BET}, was calculated according to the formula:

$$SSA = \frac{6}{d_{BET} \cdot \sum_i (\rho_i V_i)} \quad (1)$$

where ρ_i and V_i are the density and volume fraction of possible polymorphic forms, respectively. In the case of TiO_2 the calculations were carried for the following values: $\rho_{anatase}$ = 3.894 g/cm^3, ρ_{rutile} = 4.250 g/cm^3.

X – ray diffraction measurements, XRD, were performed with X'Pert MPD Philips diffractometer in Bragg – Brentano configuration. The crystallite size, d_{XRD}, was calculated according to Scherrer's formula [34].

Transmission electron microscopy, TEM, investigations were carried out using FEI TECNAI TF 20 X-TWIN (FEG) 200kV microscope.

Optical spectra of diffuse reflectance $R_{diff}(\lambda)$ were obtained with a double beam spectrophotometer Lambda 19 Perkin Elmer using integrating sphere. On the basis of these experiments fundamental band gap of TiO_2 as well as energies of optical transitions were calculated.

The electrical properties were investigated using impedance spectroscopy. The measurements were performed in air at 420°C with Solatron system (FRA 1260 + dielectric interface 1294).

Hydrogen sensing experiments consisted in measuring dynamic changes in the electrical resistance of TiO_2-based materials upon exposure to H_2. The sensors were prepared in a form of circular tablets which were formed from nanopowders by pressing under 25 MPa and subsequent heating up to 400°C for 18 h in a synthetic air atmosphere. The measurements were performed at a constant temperature chosen within the range of 200-400°C in the synthetic air working as a reference atmosphere and H_2 concentration in the range of 50 – 3000 ppm as it is described in [33].

3. Results and discussion

X – ray diffraction measurements performed for TiO_2: Cr reveal that nanomaterials are well – crystallized and two polymorphic forms, namely anatase and rutile are present as it can be concluded from Fig. 1. For the samples with 0.1 and 1 at.% Cr anatase form dominates. However, rutile fraction rises as the chromium amount increases, as it can be seen in the case of TiO_2: 5 at.% Cr.

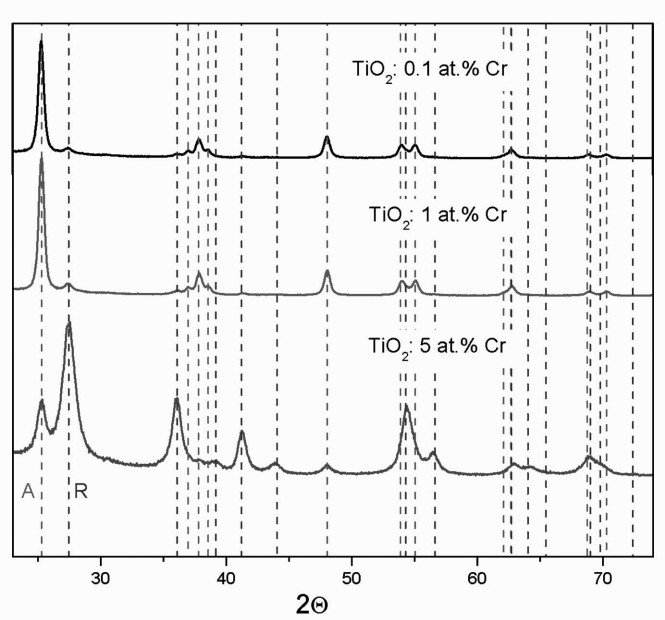

Fig. 1. XRD patterns of Cr – doped TiO_2 nanopowders; A – anatase R – rutile

Transmission Electron Microscopy, TEM, was applied to investigate morphology of TiO_2: Cr nanopowders. Fig. 2 presents selected TEM images of TiO_2: Cr nanopowders together with the grain size distributions obtained on the basis of the series of TEM results. As it can be seen, the grains of pure TiO_2 as well as those of TiO_2 doped with 0.1 and 5 at.% Cr are spherical in shape and the grain size decreases as chromium fraction rises.

TABLE 1. summarizes the results obtained from BET, XRD and TEM measurements for TiO_2 based nanostructures. As it can be seen, the intention to synthesize TiO_2: Cr with constant SSA in order to investigate the influence of Cr dopant was realized for the pure sample as well as for those doped with 0.1 and 1 at.% Cr. In the case of TiO_2: 5 at.% Cr, the obtained SSA reached 102.9 m^2/g. This effect can be attributed to the increased density of oxygen vacancies in the structure. In the literature, one can find information on *FSS* procedure to obtain TiO_2: Cr with constant *SSA* even for highly doped samples [35].

On the basis of TABLE 1. one can also observe that the crystallite size remains the same for the samples up to 1 at.% Cr, as determined from XRD measurements. No significant impact of Cr dopant on the lattice parameters *a* and *c* of TiO_2 was observed as discussed previously [28, 29]. The reason might be in the similarity between ionic radii of Cr^{3+} and Ti^{4+} which are equal to r_{Cr3+} = 0.062 nm, r_{Ti4+} = 0.061 nm, according to [36].

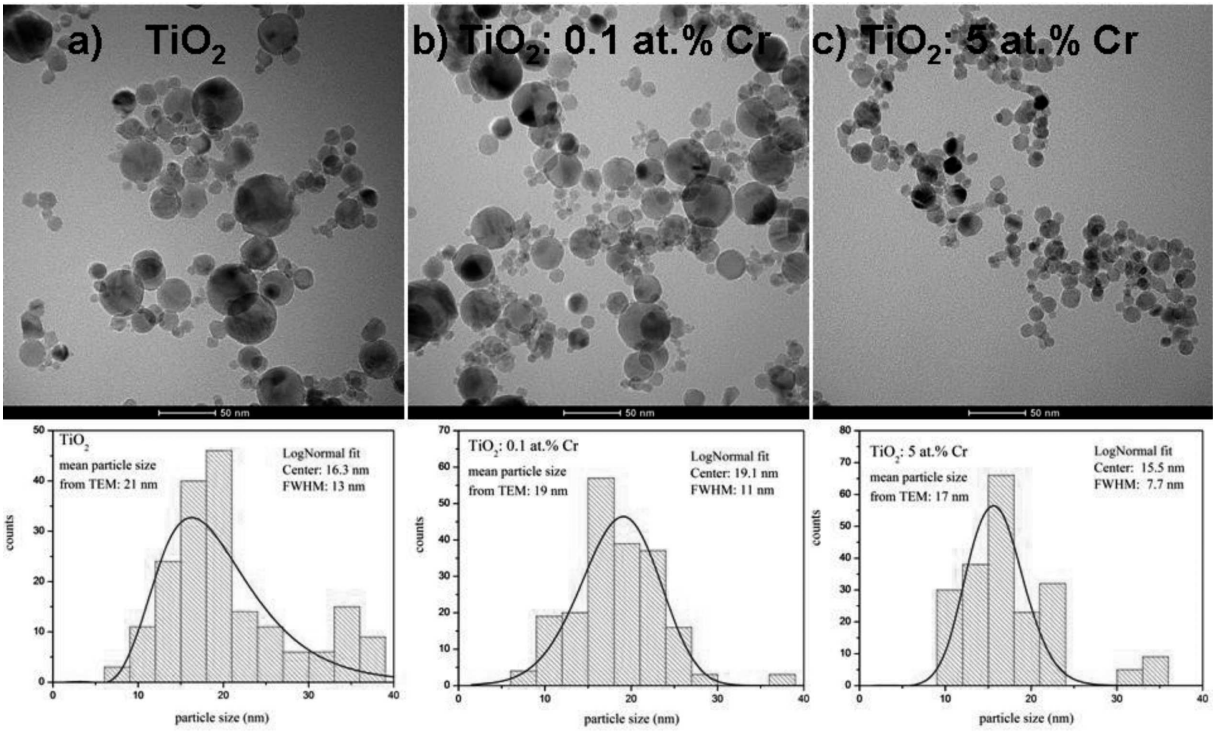

Fig. 2. TEM images of: (a) TiO_2; (b) TiO_2: 0.1 at.% Cr; (c) TiO_2: 5 at.% Cr nanopowders along with particle size distributions obtained on the basis of the series of TEM images

TABLE 1

Results of BET, XRD and TEM measurements for Cr doped TiO_2 nanopowders

at. % Cr	SSA (m^2/g)	d_{BET} (nm)	Crystallite size from XRD (nm)		Lattice parameters (nm)		Weight % of rutile	d_{TEM} (nm) mean value
			anatase (A)	rutile (R)	a	c		
0	62.7	24.5	19.9	15.9	0.3789 (A) 0.4599 (R)	0.9505 (A) 0.2957 (R)	7	21
0.1	65.3	23.5	18.6	12.2	0.3788 (A) 0.4602 (R)	0.9501 (A) 0.2958 (R)	6	19
1	60.2	25.5	18.0	12.9	0.3788 (A) 0.4598 (R)	0.9501 (A) 0.2958 (R)	6	-
5	102.9	14.0	12.1	10.9	0.3791 (A) 0.4603 (R)	0.9502 (A) 0.2953 (R)	77	17

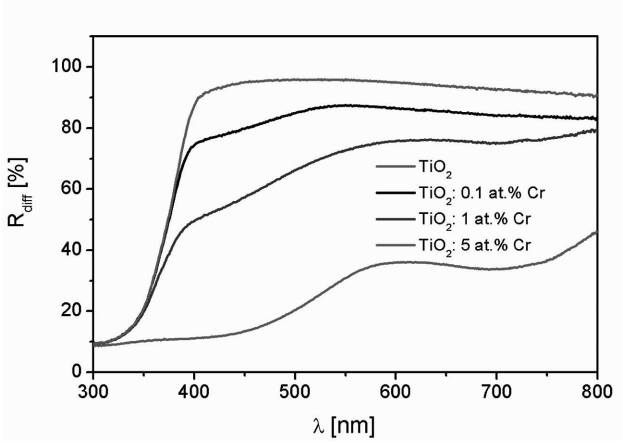

Fig. 3. Optical diffuse reflectance R_{diff} of as a function of wavelength λ obtained of TiO_2: Cr nanopowders as a function of wavelength

In order to study energies of optical transitions for the samples of TiO_2: Cr, the UV – vis spectrometry was applied. Fig. 3 demonstrates optical diffused, reflectance $R_{diff}(\lambda)$ obtained for TiO_2: Cr nanopowders with different chromium loading.

As it can be seen, the fundamental absorption edge shifts towards longer wavelengths as chromium incorporates into TiO_2 structure and forms localized acceptor levels within TiO_2 band gap. With the increasing dopant concentration, the fundamental absorption edge disappears gradually due to enlarged density of states related to the impurities in the band gap.

On the basis of the optical diffused reflectance, taking into account its derivative $dR_{Diff}/d\lambda$, one can determine energies of optical transitions corresponding to the wavelength at which the function $dR_{Diff}/d\lambda$ reaches maximum value. Fig. 4 displays the fitting procedure. For the pure TiO_2 sample there

are two optical transitions E_1 and E_2 which correspond to the band gap energies of anatase and rutile, respectively.

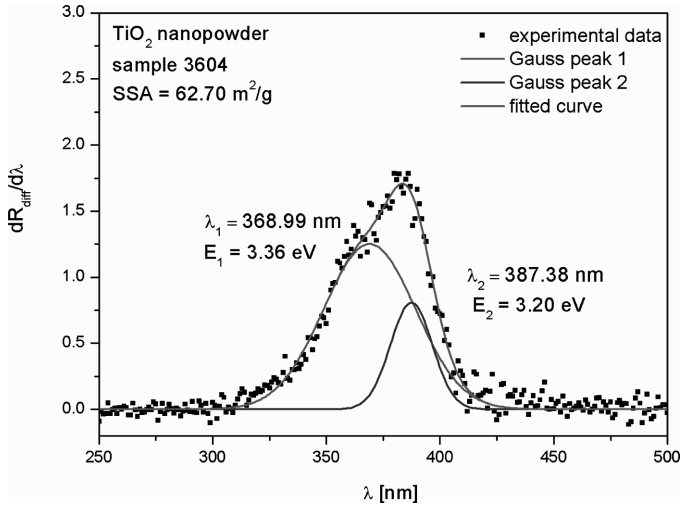

Fig. 4. Analysis of the optical transitions from reflectance spectra of TiO_2: Cr nanopowders; $dR_{diff}/d\lambda$ is the first derivative of the spectrum; λ_1 and λ_2 represent wavelengths at which $dR_{diff}/d\lambda$ attains the maximum, whereas E_1 and E_2 are energies of the optical transitions

The values of determined optical transition energies are given in TABLE 2. As one can see, the energies of optical transitions are shifted towards larger values as compared with literature data. In the case of single crystal, E is in the range of 3.20-3.26 eV for anatase and 3.02-3.05 eV for rutile [37, 38]. The observed size – dependent shift, ΔE, can be explained on the basis of quantum confinement of the charge carriers in nanometric – size grains [39]. For the sample with Cr loading equal to 5 at.%, the energies of optical transitions are not easy to distinguish. Energy E_{dop} in the range of 2.40-2.65 eV can be attributed to Cr levels [28-31].

TABLE 2
Energies of optical transitions obtained from differential reflectance spectra for TiO_2: Cr nanopowders

Sample TiO_2: Cr (at. % Cr)	E_1 (eV)	E_2 (eV)	E_{dop} (eV)
0	3.36	3.20	–
0.1	3.39	3.24	2.65
1	3.44	3.29	2.60
5	2.40		

The electrical properties of TiO_2 doped with Cr nanomaterials were investigated using impedance spectroscopy at 420°C in air. In order to study the influence of chromium dopant on the electrical conductivity, having in mind that the Specific Surface Area affects electrical properties, three samples with similar SSA were chosen. Fig. 5 presented below demonstrates the influence of Cr dopant on the impedance of TiO_2: Cr nanosensors.

As it can be seen from Fig. 5, increasing Cr concentration improves conductivity of TiO_2-based nanosensors. As chromium levels are localized relatively high above valence band (0.5-1.5 eV) of TiO_2 [28-31] it appears that in the range of temperatures below 400°C chromium is non – active dopant. Instead of ionized Cr'_{Ti} centers neutral Cr^x_{Ti}centers are formed according to the equation:

$$Cr'_{Ti} \Leftrightarrow Cr^x_{Ti} + e' \tag{2}$$

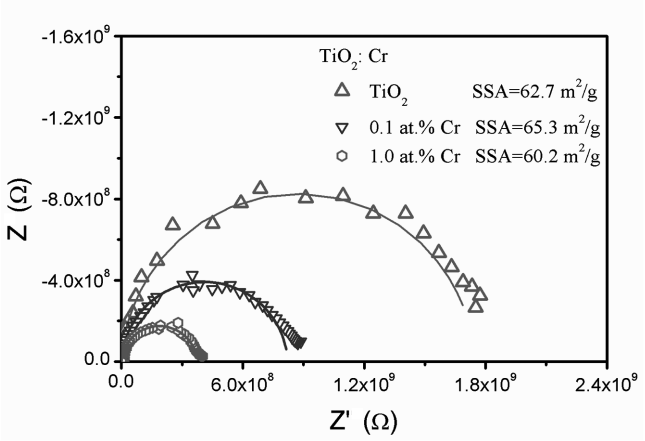

Fig. 5. Impedance spectra of TiO_2: Cr sensors with the increasing concentration of dopant measured in air at 420°C

Increasing temperature shifts the equilibrium of the above mentioned equation to the left hand side, whereas decreasing temperature promotes neutral Cr^x_{Ti} centers formation. Taking into account the reaction of Cr incorporation into TiO_2 structure:

$$Cr_2O_3 \rightarrow 2Cr'_{Ti} + 3O_O + V_O^{\bullet\bullet} \tag{3}$$

where Cr'_{Ti} represents chromium substituted in Ti position, $V_O^{\bullet\bullet}$ is an oxygen vacancy and O_O denotes oxygen at its lattice site, respectively, one can write:

$$Cr_2O_3 \rightarrow 2Cr^x_{Ti} + 3O_O + V_O^{\bullet\bullet} + 2e' \tag{4}$$

As it can be seen in this case, Cr dopant improves electrical conductivity of n – type TiO_2 nanosensor.

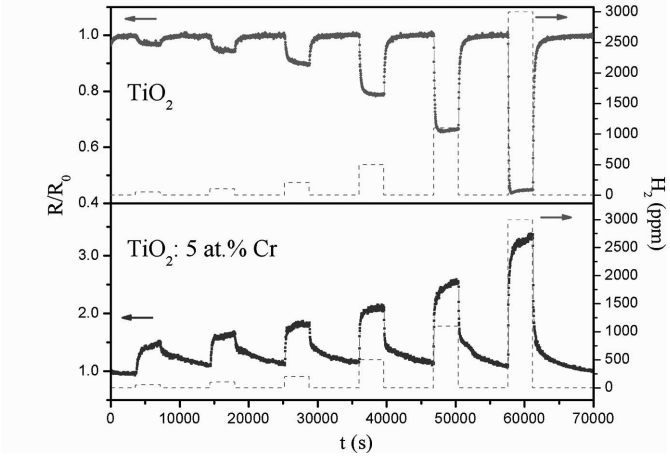

Fig. 6. Dynamic changes in the electrical resistance of TiO_2 and TiO_2: 5at.% Cr sensing tablets upon interaction with H_2 at 250°C

Fig. 6 demonstrates dynamic changes in the electrical resistance, R, of TiO_2 and TiO_2: 5 at.% Cr sensing tablets caused by interaction with hydrogen as a function of time at 250°C. The dashed, rectangular profiles in each case correspond to the step changes in hydrogen concentration in the reference atmosphere (synthetic air).

As a result of the interaction between H_2 and TiO_2 sensor, the electrical resistance, R, of pure nanomaterial decreases, whereas in the case of TiO_2: 5 at. % Cr the electrical resistance increases, which can be treated as a proof of n – p transition induced by Cr dopant. Moreover, the changes in the electrical resistance are large and reproducible.

Fig. 7 demonstrates the sensor response, S, of TiO_2 based sensors defined as R_0/R for n – type materials and R/R_0 in the case of TiO_2: 5 at.% Cr as a function of H_2 concentration at 300°C. These two definitions of the sensor response are given to facilitate interpretation and comparison between samples that exhibit n and p type conductivity. As it can be seen, 5 at.% of Cr dopant significantly improves the sensor response.

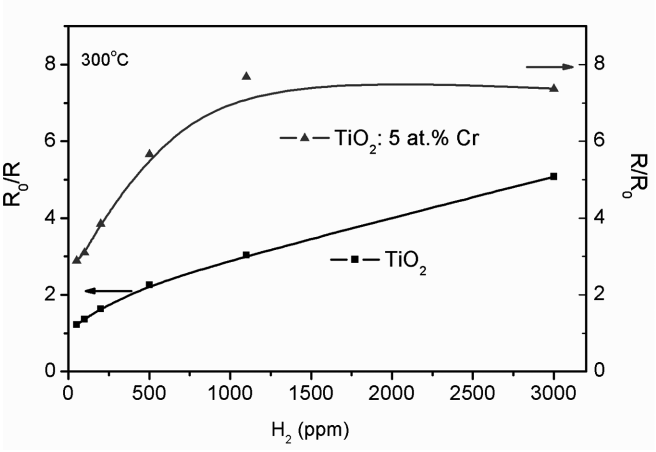

Fig. 7. Sensor response defined as R_0/R for TiO_2 (n – type sensor) and R/R_0 in the case of TiO_2: 5 at.% Cr (p – type sensor) as a function of H_2 concentration at 300°C

4. Conclusions

The results of the above – mentioned experiments on TiO_2: Cr sensors allow to draw the following conclusions:

- Flame Spray Synthesis technique enables to obtain well crystallized TiO_2 nanopowders
- Cr dopant affects anatase to rutile transformation as indicated by XRD measurements
- TEM imaging reveals that TiO_2: Cr grains are spherical in shape
- Cr additive improves conductivity of TiO_2 based materials
- The electrical resistance, R, decreases upon hydrogen exposure up to 1 at.% Cr while the reversed effect is observed at 5 at.% Cr
- Sensors obtained from TiO_2:Cr nanopowders show promising dynamic characteristics in response to hydrogen. The sensor responses are large and reproducible especially in the case of 5 at.% Cr.

Acknowledgements

One of the author (B.L-S.) acknowledges Grant for Young Scientists at the Faculty of Computer Science, Electronics and Telecommunications AGH UST. Authors would like to thank Adam Czapla and Maria Lubecka from AGH University of Science and Technology, Krakow, Poland for performing gas sensing measurements.

REFERENCES

[1] G. Pfaff, P. Reynders, Chem. Rev. **99**, 1963 (1999).
[2] J. Winkler, Titanium Dioxide, Vincentz, Hannover, 2003.
[3] A. Bozzi, T. Yuranova, I. Guasaquillo, D. Laub, J. Kiwi, J. Photochem. Photobiol. A **174**, 156 (2005).
[4] D.A. Tryk, T. Watanabe, K. Hashimoto, A. Fujishima, Internat. Glass Rev. **2**, 34 (2001).
[5] D. Alrousana, M.I. Polo-Lopez, P.S.M. Dunlop, P. Fernandez-Ibanez, J.A. Byrne, Appl. Catal. B **128**, 126 (2012).
[6] A. García, L. Delgado, J. A. Torŕ, E. Casals, E. González, V. Puntesb, X. Font, J. Carrera, A. Sánchez, J. Hazard. Mater. **199-200**, 64 (2012).
[7] A.D. Barros, K.F. Albertin, J. Miyoshi, I. Doi, J.A. Diniz, Microelectron. Eng. **87**, 443 (2010).
[8] T. Bansal, C.A. Durcan, N. Jain, R.B. Jacobs-Gedrim, Y. Xu, B. Yu, Carbon **55**, 168 (2013).
[9] Q. Chaudhry, L. Castle, Trends Food Sci. Technol. **22**, 595 (2011).
[10] K. Siwińska-Stefańska, M. Nowacka, A. Kołodziejczak-Radzimska, T. Jesionowski, Dyes and Pigments **94**, 338 (2012).
[11] H. Wang, H. Li, J. Wang, J. Wu, Mater. Lett. **80**, 99 (2012).
[12] E. Le Boulbar, E. Millon, E. Ntsoenzok, B. Hakim, W. Seiler, C. Boulmer-Leborgne, J. Perriere, Opt. Mater. **34**, 1419 (2012).
[13] M. Ilie, B. Cojocaru, V.I. Parvulescu, H. Garcia, Int. J. Hydrogen Energy **36**, 15509 (2011).
[14] R. Xiong, G. Sang, X. Yan, G. Zhang, X. Ye, C. Jiang, L. Luo, Int. J. Hydrogen Energy **37**, 10222 (2012).
[15] S. Songara, M.K. Patra, M. Manoth, L. Saini, V. Gupta, G.S. Gowd, S.R. Vadera, N. Kumar, J. Photochem. Photobiol. A **209**, 68 (2010).
[16] A.Z. Sadek, J.G. Partridge, D.G. McCulloch, Y. X. Li, X. F. Yu, W. Wlodarski, K. Kalantar-zadeh, Thin Solid Films **518**, 1294 (2009).
[17] Y. Kimura, S. Kimura, R. Kojima, M. Bitoh, M. Abe, M. Niwano, Sens. Actuators B **177**, 1156 (2013).
[18] H. Jamil, S.S. Batool, Z. Imran, M. Usman, M.A. Rafiq, M. Willander, M.M. Hassan, Ceram. Int. **38**, 2437 (2012).
[19] G. Neri, A. Bonavita, S. Galvagno, Y. X. Li, K. Galatsis, W. Wlodarski, IEEE Sens. J. **3**, 195 (2003).
[20] M. Ferroni, M.C. Carotta, V. Guidi, G. Martinelli, F. Ronconi, O. Richard, D.V. Dyck, J.V. Landuyt, Sens. Actuators B **68**, 140 (2000).
[21] R.K. Sharma, M.C. Bhatnagar, G.L. Sharma, Sens. Actuators B **45**, 209 (1997).
[22] K. Zakrzewska, M. Radecka, M. Rekas, Thin Solid Films **310**, 161 (1997).
[23] A. Ruiz, G. Sakai, A. Cornet, K. Shimanoe, J. Morante, N. Yamazoe, Sens. Actuators B **93**, 509 (2003).
[24] M. Radecka, M. Rekas, Solid State Phenom. **39-40**, 135 (1994).
[25] S. Karvinen, Solid State Sci. **5**, 811 (2003).
[26] C.C. Tsai, H. Teng, Appl. Surf. Sci. **254**, 4912 (2008).
[27] D.A. Hanaor, C.C. Sorrell, J. Mater. Sci. **46**, 855 (2011).
[28] M. Radecka, K. Zakrzewska, M. Wierzbicka, A. Gorzkowska, S. Komornicki, Solid State Ionics **157**, 379 (2003).
[29] K. Wilke, H.D. Breuer, J. Photochem. Photob. A **121**, 49 (1999).
[30] J.L. Carpentier, A. Lebrun, F. Perdu, J. Phys. Chem. Solids **50**, 145 (1989).
[31] T.H. Jun, K.S. Lee, Mater. Lett. **64**, 2287 (2010).
[32] I. Alessandri, E. Comini, E. Bontempi, G. Faglia, L.E. Depero, G. Sberveglieri, Sens. Actuators B **128**, 312 (2007).

[33] B. Lyson-Sypien, A. Czapla, M. Lubecka, P. Gwizdz, K. Schneider, K. Zakrzewska, K. Michalow, T. Graule, A. Reszka, M. Rekas, A. Lacz, M. Radecka, Sens. Actuators B **175**, 163 (2012).
[34] B.D. Cullity, Elements of X – ray Diffraction, Reading UK, Addison – Wesley, 1978.
[35] K.A. Michalow, E.H. Otal, D. Burnat, G. Fortunato, H. Emerich, D. Ferri, A. Heel, T. Graule, Catal. Today **209**, 47 (2012).
[36] R.D. Shannon, Acta Crystallogr. A **32**, 751 (1976).
[37] S.D. Mo, W.Y. Ching, Phys. Rev. B **46**, 13023 (1995).
[38] H. Tang, H. Berger, P.E. Schmid, F. Levy, Solid State Commun. **92**, 267 (1994).
[39] M. Radecka, M. Rekas, E. Kusior, K. Zakrzewska, A. Heel, K.A. Michalow, T. Graule, J. Nanosci. Nanotechnol. **10**, 1032 (2010).

Received: 20 February 2014.